Inelastic transverse magnetic dipole electron scattering form factors in ^{48}Ca (restricted optimum configurations)

Firas Z. Majeed, Redhab A. Allawe

Department of Physics, Collage of Science, Baghdad University, Baghdad, Iraq

E-mail: abosajjad_altameme@yahoo.com

Abstract

Inelastic transverse magnetic dipole electron scattering form factors in ^{48}Ca have been investigated through nuclear shell model in an excited state energy Ex= 10.23 MeV which is so called "mystery case" with different optional choices like effective interaction, restricted occupation and core polarization interaction. ^{40}Ca as an inert core will be adopted and four orbits with eight particles distributed mainly in 2p1f model space and in some extend restricted to make sure about the major accuse about this type of transition. Theoretical results have been constituted mainly with experimental data and compared with some important theoretical results of the same transition.

Key words

Magnetic dipole moment, ^{48}Ca, electron scattering form factors.

Article info.

Received: Sep. 2015
Accepted: Dec. 2015
Published: Sep. 2016

عوامل التشكل للاستطارة الإلكترونية المستعرضة المغناطيسية غير المرنة ثنائيه القطب في نواه ^{48}Ca (التشكيلات المقيدة الفضلى)

فراس زهير مجيد، رضاب عباس علاوي

قسم الفيزياء، كلية العلوم، جامعة بغداد، بغداد، العراق

الخلاصة

تم التحقق عن عوامل التشكل للاستطارة الالكترونية المستعرضة المغناطيسية غير المرنة ثنائي القطب لنواة ^{48}Ca، وذلك من خلال أنموذج القشرة وبطاقـــة تهيج Ex= 10.23 MeV المعروفة بـ (الحالة المبهمة) مع خيارات اختياريه مختلفة مثل:- التفاعل الفعال، الاحتلالات الانتقائية وتفاعلات استقطاب القلب الخامل. اعتُمدت نواة ^{40}Ca كقلب خامل مع أربع أغلفة وثمانية جسيمات تتوزع بصورة رئيسية في أنموذج الفضاء (2p1f) مع بعض الأغلفة الممتدة المنتقاة لكي يتم التأكد من الحالة الرئيسية لهذا النوع من الانتقال. النتائج النظرية تم تشكيلها و مقارنتها مع بعض القيم التجريبية النظرية لنفس الانتقال.

Introduction

In order to understand the nuclear forces and the laws that control the interactions of elementary particles, the scattering of variety of particles by a variety of targets is the only available technique [1].

The scattering of electrons from the nuclei at high energies has provided important information about the size of nucleus, radial shape of the charge distribution, current and magnetization densities involved in the transition. Also, the electron acts as a good probe for measuring the size of the nucleus[1]. In electron scattering one can directly relate the cross section to the transition matrix elements of the local charge and current density operators and consequently directly related to the structure of the target nucleus itself [1].

The calculation of the scattering cross section, for a relativistic electron from spineless nuclei of charge Ze, was performed by Mott in 1929 [2]. The nuclear size can be taken into

account by multiplying the Mott's cross section by a factor that depends on the charge, current and magnetization distributions in the target nucleus, this factor is called "Nuclear Form Factor".

Backward-angle high-resolution inelastic electron scattering on $^{40,42,44,48}Ca$ and observation of a very strong magnetic dipole ground-state transition in ^{48}Ca had been carried out by Steffen et al. in (1980) [3]. They described magnetic dipole transitions from the ground state-even Ca isotopes to high lying $J^{\pi} = 1^{+}$ states by means of low momentum transfer but high resolution inelastic electron scattering.

Electron scattering form factor for (10.23 MeV) excitation in ^{48}Ca has been studied by Burt et al. in (1982)[4], they use of the technique of Second order perturbation Random Phase Approximation (SRPA + Δ-hole excitation) used between the two particle-two hole states with (4ħω) excitation and their results were in a good agreement with the experimental data.

Takayanagy et al. in (1988) [5] through their theoretical study of magnetic dipole transition in ^{48}Ca has been calculated the form factor of M1 transition and using of Random Phase Approximation technique (RPA) in the 0ħω and 4ħω (2p-2h) with Δ-hole, meson exchange, configuration space, and response function analysis, and they compared the results with the experimental data.

Shell-model plus Hartree - Fock calculations for the neutron-rich Ca isotopes have been studied by Brown and Richter in (1998) [6] including comparative study with the result of experimental inelastic electron scattering form factor (M1) in ^{48}Ca, they used the model space effective interaction FPD6+ HF large basis, the results were not coinciding with the experimental data.

Richter in (2005) [7] through his work on magnetic dipole and Gamow-Teller modes: quenching, fine structure and astrophysical implications demonstrated that high-precision M1 data on N = 28 isotones from electron scattering at Darmstadt permit the extraction of neutral-current neutrino-nucleus scattering cross sections important for supernova dynamics and nucleosynthesis, by the use of the technique RPA and he modified his theory by the use of SRPA +(π+ ρ) meson exchange between the two particle -two hole states with 4ħω excitation and his results are nearly in a good agreement with the experimental data.

In the present work, the core polarization effects with higher configuration in the first order perturbation theory and the two-body matrix elements and the detection of the suitable transition from the magnetic dipole transition (M1 transition) for ^{48}Ca will be introduced. Harmonic oscillator (HO) single-particle basis had been used. A computer program is written in FORTRAN 90 language to include realistic interaction the Michigan three Yukawa (M3Y) in the original code to calculate the model space form factors (zero-order) and the first-order core polarization effects. This code was written by Prof. R .A .Radhi.

Theory

The reduced matrix elements for a selected operator T^{η}_{JT} are written as the sum of the product of the one-body transition density matrix elements (OBDM) times the single-particle transition matrix elements [8] :

$$\left\langle \Gamma_f \left\| \hat{T}^{\eta}_{\Lambda} \right\| \Gamma_i \right\rangle = \sum_{\alpha,\beta} OBDM\left(\Gamma_i, \Gamma_f, \alpha, \beta\right) \left\langle \alpha \left\| \hat{T}^{\eta}_{\Lambda} \right\| \beta \right\rangle \quad (1)$$

where $\Lambda = JT$ is the multipolarity and the states $\Gamma_i \equiv J_i T_i$ and $\Gamma_f \equiv J_f T_f$ are initial and final states of the

nucleus. While α and β denote the final and initial single-particle states, respectively (isospin is included).

The reduced matrix elements of the electron scattering operator $\hat{T}_\Lambda^\eta$ consist of two parts, one is for the "Model space" matrix elements, and the other is for the "Core-polarization" matrix elements [9].

$$\left\langle \Gamma_f \left\| \hat{T}_\Lambda^\eta \right\| \Gamma_i \right\rangle = \left\langle \Gamma_f \left\| \hat{T}_\Lambda^\eta \right\| \Gamma_i \right\rangle_{MS} + \left\langle \Gamma_f \left\| \delta\hat{T}_\Lambda^\eta \right\| \Gamma_i \right\rangle_{CP} \quad (2)$$

where

$\left\langle \Gamma_f \left\| \hat{T}_\Lambda^\eta \right\| \Gamma_i \right\rangle_{MS}$ are the model-space matrix elements,

$\left\langle \Gamma_f \left\| \delta T_\Lambda^\eta \right\| \Gamma_i \right\rangle_{CP}$ are the core- polarization matrix elements.

$\left|\Gamma_i\right\rangle$ and $\left|\Gamma_f\right\rangle$ are described by the model-space wave functions.

The core-polarization matrix element can be written as follows [9]:

$$\left\langle \Gamma_f \left\| \delta\hat{T}_\Lambda^\eta \right\| \Gamma_i \right\rangle_{cp} = \sum_{\alpha,\beta} OBDM(\alpha,\beta) \left\langle \alpha \left\| \delta\hat{T}_\Lambda^\eta \right\| \beta \right\rangle_{cp} \quad (3)$$

According to the first order perturbation theory, the single-particle matrix element for the higher-energy configurations is given by [8] :

$$\langle a|\delta\hat{T}_J^\eta|b\rangle = \langle a|V_{res}\frac{Q}{E-H^{(0)}}\hat{T}_J^\eta|b\rangle + \langle a|\hat{T}_J^\eta\frac{Q}{E-H^{(0)}}V_{res}|b\rangle \quad (4)$$

where V_{res} are adopted here as a residual nucleon-nucleon interaction. The single-particle energies are calculated according to the following equation [8]:

$$e_{nlj} = (2n+l-\tfrac{1}{2})\hbar\omega + \begin{cases} -\frac{1}{2}(l+1)\langle f(r)\rangle_{nl} & for\ j=l-\frac{1}{2} \\ \frac{1}{2}l\langle f(r)\rangle_{nl} & for\ j=l+\frac{1}{2} \end{cases} \quad (5)$$

with

$$\left\langle f(r)\right\rangle_{nl} \approx 20\ A^{-2/3}\ MeV$$

$$\hbar\omega = 45\ A^{-1/3} - 25\ A^{-2/3} \quad (6)$$

The transverse form factor arises from the interaction of the electron with the current $\vec{J}(\vec{r},t_z)$, and the magnetization distributions $\vec{\mu}(\vec{r},t_z)$ of the nucleus. The magnetic operator is given by [10]

$$\hat{T}^m_{JM,t_Z}(q) = \int \vec{dr}\vec{M}_{JLM}(q,r)\cdot\vec{J}(\vec{r},t_z) \quad (7)$$

with

$$\vec{M}_{JLM}(q,\vec{r}) = j_L(qr)\vec{Y}_{JL1M}(\Omega_r) \quad (8)$$

For the two-body matrix elements of the residual interaction $\langle \alpha\alpha_2|V_{res}|\beta\alpha_1\rangle_\Gamma$, which appear in Eq.(4), M3Y interaction of Nakada et. al [1] is adopted. This interaction was given in LS-coupling and tensor force, density dependence part which calculates the zero range term.

A transformation between LS and jj must be performed to get the relation between the two-body shell model matrix elements and the relative and center of mass coordinates, using the harmonic oscillator radial wave functions with Brody-Moshinsky transformation.

The realistic M3Y effective NN interaction, which is used in electron scattering (V_{res}) is expressed as a sum of the central potential part, spin-orbit potential part, and long range tensor part, as follows [12]:

$$V_{res} = V_C + V_{ten} + V_{s.l} + V_{DD} \quad (9)$$

the four potentials are expressed as [12]:-

$$V_{12}^{(C)} = \sum_n (t_n^{(SE)}P_{SE} + t_n^{TE}P_{TE} + t_n^{(SO)}P_{SO} + t_n^{(To)}P_{TO}) f_n^{(c)}(r_{12})$$

$$V_{12}^{(LS)} = \sum_n (t_n^{(LSE)}P_{TE} + t_n^{(LSO)}P_{TO}) f_n^{(LS)}(r_{12}) L_{12}(\vec{S}_1 + \vec{S}_2)$$

$$V_{12}^{(TN)} = \sum_n (t_n^{(TNE)}P_{TE} + t_n^{(TNO)}P_{TO}) f_n^{(TN)}(r_{12}) r_{12}^2 S_{12}$$

$$V_{12}^{(DD)} = t^{(DD)}\{(1-x^{(DD)})P_{SE} + t_n^{(DD)}(1+x^{(DD)})P_{TE})\}\delta^{(TN)}(r_{12}) \quad (10)$$

The values of the best fit to the potential parameters are showed in Table 1.

Table 1: The values of the best fit to the potential parameters [13].

Parameters	Unit	M3Y-P0	M3Y-P1	M3Y-P2
$R_1^{(C)}$	fm	0.25	0.25	0.25
$t_1^{(se)}$	MeV	11466	8599.5	8027
$t_1^{(Te)}$	MeV	13967	10475.25	6080
$t_1^{(so)}$	MeV	-1418	-1418	-11900
$t_1^{(To)}$	MeV	11345	11345	3800
$R_2^{(C)}$	fm	0.40	0.40	0.40
$t_2^{(se)}$	MeV	-3556	-3556	-3556
$t_2^{(so)}$	MeV	-4594	-4594	-4266
$t_2^{(Te)}$	MeV	950	950	1730
$t_2^{(To)}$	MeV	-1900	-1900	-780
$R_3^{(C)}$	fm	1.414	1.414	1.414
$t_3^{(se)}$	MeV	-10.463	-10.463	-10.463
$t_3^{(so)}$	MeV	-10.463	-10.463	-10.463
$t_3^{(Te)}$	MeV	31.389	31.389	31.389
$t_3^{(To)}$	MeV	3.488	3.488	3.488
$R_1^{(LS)}$	fm	0.25	0.25	0.25
$t_1^{(Lse)}$	MeV	-5101	-9181.8	-9181.8
$t_1^{(Lso)}$	MeV	-1897	-3414.6	-3414.6
$R_2^{(LS)}$	fm	0.40	0.40	0.40
$t_2^{(Lse)}$	MeV	-377	-606.6	-606.6
$R_1^{(LS)}$	Fm	1.414	1.414	1.414
$t_3^{(Lse)}$	MeV	0	0	0
$t_3^{(Lso)}$	MeV	0	0	0
$R_1^{(TN)}$	fm	0.4	0.4	0.4
$t_1^{(TNE)}$	(MeV fm^{-2})	-1096	-131.52	-131.52
$t_1^{(TNO)}$	(MeV fm^{-2})	244	29.28	29.28
$R_2^{(TN)}$	fm	0.70	0.70	0.70
$t_2^{(TNE)}$	(MeV fm^{-2})	-30.9	-3.708	-3.708
$t_2^{(TNO)}$	(MeV fm^{-2})	15.6	1.872	1.872
$R_3^{(TN)}$	fm	1.414	1.414	1.414
$t_3^{(TNE)}$	(MeV fm^{-2})	0.0	0.0	0.0
$t_3^{(TNO)}$	(MeV fm^{-2})	0.0	0.0	0.0
$t_{DD}^{(se)}$	(MeV fm)	0.0	1092	181
$t_{DD}^{(TE)}$	(MeV fm)	0.0	1331	1139

Results and discussion

The concept of the core-polarization effects has been introduced in order to account for the participation of configurations from outside of the model space in the transition.

because of the mystery inherent with the measurements of the properties like magnetic moments, β-decay and Gamow-Teller GT transition and these properties need to be corrected by different approaches including the use of first order configuration mixing through first order perturbation theory where the core is included to the calculations beside the use of well-

defined model space, so we shall introduce the most important result obtained for this types of transition.

The nucleus ^{48}Ca is the lightest doubly magic nucleus with a neutron excess. It is known to be a good shell-model nucleus and thus provides an excellent testing ground for nuclear models. In fact, the nucleus ^{48}Ca is more inert than ^{40}Ca, ^{48}Ni and ^{56}Ni because of the closed sub shell neutron $1f_{7/2}$ so that it is an interesting one in fp shell nuclei. We use the single particle wave functions of the HO with size parameter b= 1.988 fm.

The model spaces is adopted in this work which is fp shell model space for ^{48}Ca. Core-polarization effects are taken into account through first order perturbation theory, which allows particle-hole excitation from shell core orbits $1s_{1/2}$, $1p_{3/2}$, $1p_{1/2}$, $1d_{5/2}$, $1d_{3/2}$and $2S_{1/2}$(shell model space having ^{40}Ca as an inert core) to all higher orbits with $2\hbar\omega$ excitation for normal transitions. The model space effective interaction FPD6 [14, 15] has been used to give the ($1f_{7/2}1f_{5/2}2p_{3/2}2p_{1/2}$) shell model wave functions for ^{48}Ca. The OBDM elements for all transitions considered are given in Table 2 and will be referred to subsequently as each form factor is to be considered in turn.

Table 2: The OBDM elements for all cases.

Cases	J_i	J_f	OBDM (ΔT=0))	OBDM (ΔT=1))
Case1 1^+_3	7/2	7/2	0.45534	0.29392
	5/2	5/2	-0.70542	-0.45534
Case2 1^+_1	7/2	7/2	-0.03403	-0.02196
	3/2	3/2	-1.02469	-0.66144
	5/2	5/2	0.78659	0.50774
	1/2	1/2	-1.10129	-0.71088
Case3 1^+_2	3/2	3/2	0.94541	0.61026
	5/2	5/2	-0.50534	-0.32620
Case4 1^+_2	7/2	7/2	0.21107	0.13625
	3/2	3/2	0.59595	0.38468
	5/2	5/2	-0.64554	-0.41670
Case5 1^+_1	7/2	7/2	0.66335	0.42819
	5/2	5/2	-1.23013	-0.79405
	1/2	1/2	1.19781	0.77318
Case6 1^+_1	3/2	3/2	1.27576	0.82350
	5/2	5/2	-0.86479	-0.55822
	1/2	1/2	1.08183	0.69832

For M1 transverse magnetic form factor, there are many cases in which the eight neutrons distributed mainly in the model space $1f_{7/2}$, $2p_{3/2}$, $1f_{5/2}$, $1p_{1/2}$ (^{40}Ca as an inert core). In all cases the inelastic transverse form factors (M1) have been calculated using M3Y-P2. the experimental data for all cases are taken from Ref. [16] and these cases are:-

1. Case1- $|f_{7/2}^5 p_{3/2}^0 f_{5/2}^1 p_{1/2}^2 : 1^+ 4\rangle$

Fig. 1 represents the (1^+_3) transition, the core curve is lower than the model space and total form factor curves, then the core part have a positive contribution. The calculated form factor which is a homogenous curve, goes underestimated and near from experimental data with (0.025) $F|q|^2$ different between them for the first

peak, but at q=0.9 fm^{-1} the calculated result is closer to experimental data in value but overestimate the experimental value. At (q>1), the results underestimate the experimental data and deviate from the peak and goes down at q=1.2 fm^{-1}. The value of B(M1) is far from experimental value $B(M1)_{EXP}$=3.9±0.3 $(n.m)^2$ [17] which is equal to 1.653 $(n.m)^2$. For all other cases, they have the same experimental value of B(M1).

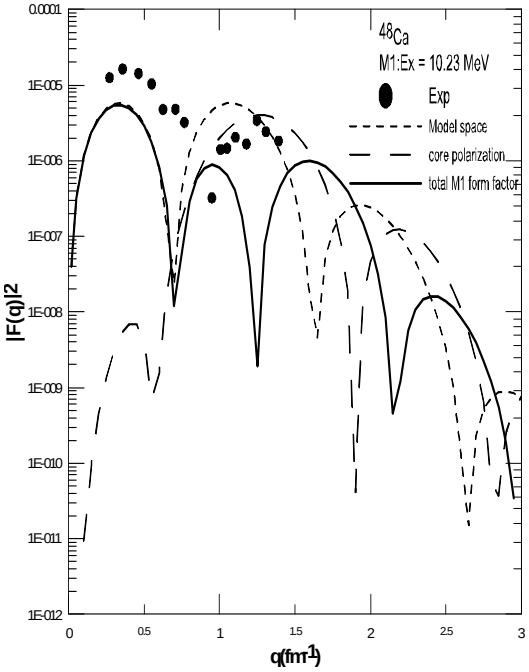

Fig. 1: Inelastic transverse M1 form factors for the first case in ^{48}Ca.

2. Case2- $|f_{7/2}^4 p_{3/2}^2 f_{5/2}^1 p_{1/2}^1 : 1^+ 4>$

Fig. 2 represents the (1^+_1) transition, the core curve is lower than the model space and total form factor curves, then the core part have a positive contribution. The calculated form factor which is a ripple curve, goes near the experimental data and underestimated at q between (0.1_0.7)fm^{-1}, but at q=(0.7_1.25) fm^{-1} the calculated result is overestimated and closer to experimental data in value and but not coincide with it except at q=(0.75_1.25) fm^{-1}. At (q>1.25) fm^{-1}, the results underestimate the experimental data and deviate from the peak. In this case, the value of B(M1) increase as compared with Previous case but still far from experimental value which is equal to 2.357 $(n.m)^2$.

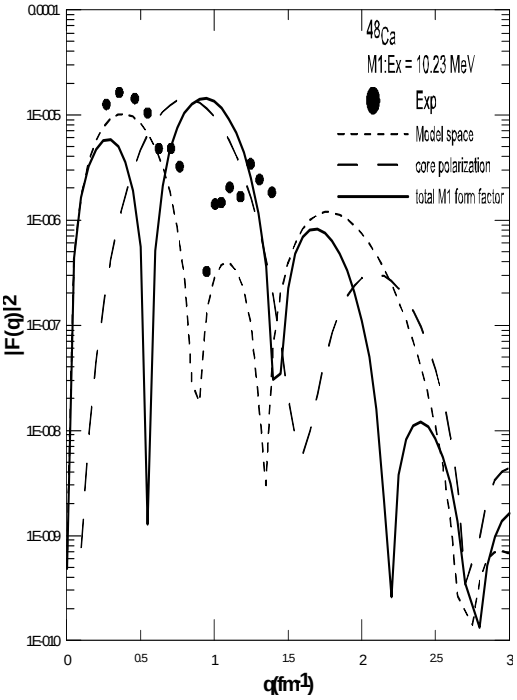

Fig. 2: Inelastic transverse M1 form factors for the second case in ^{48}Ca.

3. Case3- $|f_{7/2}^0 p_{3/2}^3 f_{5/2}^3 p_{1/2}^2 : 1^+ 4>$

Fig. 3 represents the (1^+_2) transition, the core curve is lower than the model space and total form factor curves, then the core part have a positive contribution. The calculated form factor which is a ripple curve, goes far from experimental data with (0.03) $F|q|^2$ different between them for the first peak, but at q=(0.6_1.25) fm^{-1}, the calculated result is close to the experimental data and overestimated but not coincide with it except at q=(0.6,1.25)fm^{-1}. At (q>1.25) the results underestimate the experimental data and deviate from the peak because the wave function of the harmonic oscillator. For this case, the value of B(M1) increase as compared with previous cases but still far from experimental value which is equal to 2.37 $(nm)^2$.

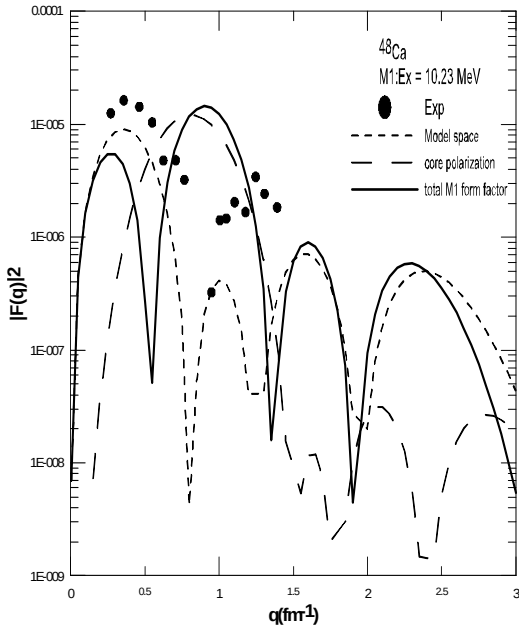

Fig. 3: Inelastic transverse M1 form factors for the third case in ^{48}Ca.

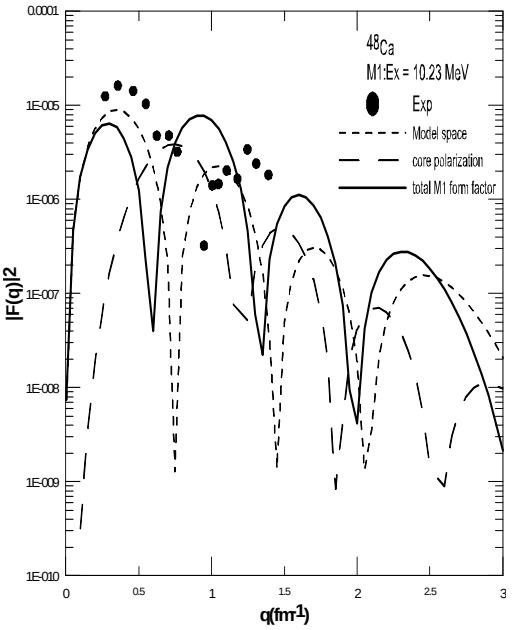

Fig. 4: Inelastic transverse M1 form factors for the fourth case in ^{48}Ca.

4. Case4- $|f_{7/2}^{1}p_{3/2}^{2}f_{5/2}^{5}p_{1/2}^{0}:1^{+}4>$

Fig. 4 represents the (1^{+}_{2}) transition, the core curve is lower than the model space and total form factor curves, then the core part have a positive contribution. The calculated form factor which is a homogenous curve, goes underestimated at all regions and far from experimental data with (0.025) $F|q|^2$ different between them for the first peak, but at q=(0.75_1.2) fm^{-1}, the calculated result goes closer from experimental data and overestimated and coincide with it very much. At (q>1.25), the results underestimate the experimental data and deviate from the peak and goes down at q=1.4 fm^{-1}. The value of B(M1) increase than the previous cases but still far from experimental value which is equal to 2.449 $(nm)^2$.

5. Case5- $|f_{7/2}^{1}p_{3/2}^{4}f_{5/2}^{2}p_{1/2}^{1}:1^{+}4>$

Fig. 5 represents the (1^{+}_{1}) transition, the core curve is lower than the model space and total form factor curves, then the core part have a positive contribution. The calculated form factor which is a ripple curve, goes near from experimental data at q between (0.1_1) fm^{-1} and underestimated but at q=1fm^{-1}, the calculated result goes closer from experimental data and overestimated but not coincide with it. At(q>1) the results underestimate the experimental data and deviate from the peak. The value of B(M1) increase than the previous cases but still far from experimental value which is equal to 2.65 $(nm)^2$.

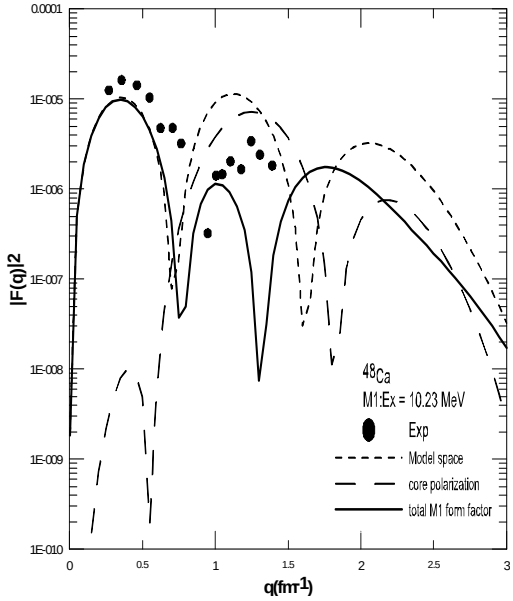

Fig. 5: Inelastic transverse M1 form factors for the fifth case in ^{48}Ca.

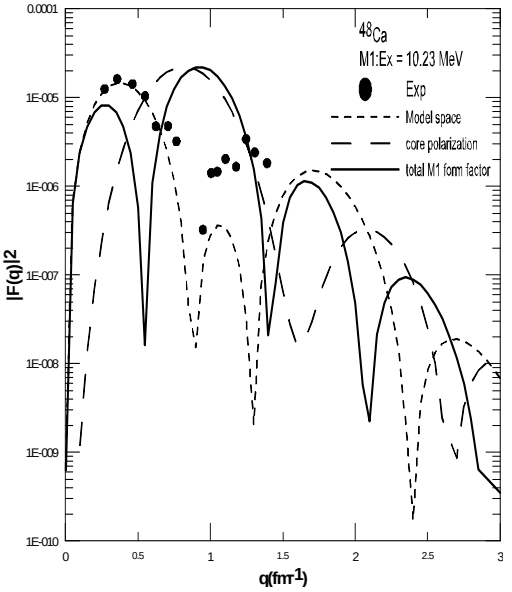

Fig. 6: Inelastic transverse M1 form factors for the sixth case in ^{48}Ca.

6. Case6- $|f_{7/2}^{0}p_{3/2}^{2}f_{5/2}^{5}p_{1/2}^{1}:1^{+}4>$

Fig. 6 represents the (1^{+}_{1}) transition, the core curve is lower than the model space and total form factor curves, then the core part have a positive contribution. The calculated form factor which is a ripple curve, goes so near the experimental data and underestimated with (0.01) F|q|2 different between them for the first peak, but at q=(0.75_1.25) fm^{-1} the calculated result is close to the experimental data and overestimated but not coincide with it except at q=(0.75_1.25) fm^{-1}. This figure shows the best fit between the calculated result and experimental data between the previous figures. For the case, the value of B(M1) have the best fit with experimental value {$B(M1)_{EXP}$=3.9±0.3 $(n.m)^2$} between the previous cases which is equal to 3.427 $(nm)^2$.

Table 3: The values of B(M1) for all cases.

CASES	BM1 in $(n.m)^2$ unit
CASE 1 1^{+}_{3}	1.653
CASE2 1^{+}_{1}	2.357
CASE3 1^{+}_{3}	2.37
CASE 4 1^{+}_{2}	2.449
CASE 5 1^{+}_{1}	2.65
CASE 6 1^{+}_{1}	3.427

Conclusions

1- Restricted occupations make the resulted form factors more ripples and far from accurate geometries.
2- Evacuation of $1f_{7/2}$ orbit makes the (BM1) more accurate than the others.
3- For all of the sixth selected occupations, the core parts are in positive contributions.
4- Best restricted occupation is $|f_{7/2}^{0}p_{3/2}^{2}f_{5/2}^{5}p_{1/2}^{1}:1^{+}4>$.

Acknowledgement

The authors are very grateful to Prof. Dr. Raad A. Radhi for his assistance and providing the original copy of two codes used for calculation the form factors and residual interaction.

References

[1] Stephen Gasiorowicz; "Quantum Physics" 2nd ed. (1995) 387.
[2] N.F.Mott., Proc.Roy.Soci.Ser, A124 (1929) 425.
[3] W. Steffen, H. D. Gräf, W. Gross, D. Meuer, A. Richter, E. Spamer, O. Titze, W. Knüpfer, Phys. Lett. B95 (1980) 23.
[4] P. E. Burt, L. M. Fagg, H. Cranell, D. I. Sober, K. J. Stapor, J. T. O'Brien, K. M. Maruyama, J. W. Lightbody, R. A. Lindgren, Phys. Rev. C28 (1982) 2805.
[5] K. Takayanagi, K. Shimizu, A. Arima, Nucl. Phys. A481 (1988) 313.
[6] A. Brown and A. Richter, Phys. Rev. C58 (1998) 2099.
[7] A. Richter, Jour. of Phys. Conf. Series, 20 (2005) 13.
[8] P.J. Brussaard and P. W. M. Glademans, "Shell-model Application in Nuclear Spectroscopy", North-Holland Publishing Company, Amsterdam (1977).
[9] R. A. Radhi, A. Bouchebak, Nucl. Phys. A716 (2003) 87.
[10] T. de Forest and J.D.Walecka, Adv. Phys., 15 (1966) 1.
[11] R.A. Radhi, A.A. Abdullah, Z.A. Dakhil, N.M. Adeeb, Nucl. Phys. A696 (2001) 442.
[12] B. A. Brown, R. A. Radhi, B. H. Wildenthal, Phys. Rev. C101 (1983) 314.
[13] H.Nakada, Phys. Rev. C, 78, (2008) 054301
[14] W. A. Richter, M. G. Van der Merwe, R. E. Julies, B. A. Brown, Nucl. Phys. A577 (1994) 585.
[15] T. Mizusaki, T. Otsuka, Y. Utsoni, M. Honma, T. Sebe, Phys. Rev. C59 (1999) R1846.
[16] J. E. Wise, J. S. Mc Carthy, R. Altemus, B. E. Norum, R. R. Whitney, J. Hiesenberg, J. Dawson, O. Schwentker, Phys. Rev. C31 (1985) 1699.
[17] W. Steffen, H. D. Gräf, W. Gross, D. Meuer, A. Richter, E. Spamer, O. Titze, W. Knüpfer, Phys. Lett. B95 (1980) 23.